

Building topological device through emerging robust helical surface states

Zibo Wang,^{1,2} Juntao Song,³ Haiwen Liu,^{1,2} Hua Jiang,^{4,*} and X. C. Xie^{1,2}

¹International Center for Quantum Materials, Peking University, Beijing 100871, China

²Collaborative Innovation Center of Quantum Matter, Beijing 100871, China

³Department of Physics, Hebei Normal University, Hebei 050024, China

⁴Department of Physics, Soochow University, Suzhou 215006, China

(Dated: May 6, 2021)

We propose a nonlocal manipulation method to build topological devices through emerging robust helical surface states in $Z_2 = 0$ topological systems. Specifically, in a ribbon of $Z_2 = 0$ Bernevig-Hughes-Zhang (BHZ) model with finite-size effect, if magnetic impurities are doped on the top (bottom) edge, the edge states on the bottom (top) edge can be altered according to the strengths and directions of these magnetic impurities. Consequently, the backscattering between the emerging robust helical edge states and gapped normal edge states due to finite-size confinement is also changed, which makes the system alternate between a perfect one-channel conductor and a perfect insulator. This effect allows us to fabricate topological devices with high on-off ratio. Moreover, it can also be generalized to 3D model and more realistic Cd_3As_2 type Dirac semimetals.

PACS numbers: 72.25.Dc, 73.20.-r, 73.43.-f, 73.63.-b

I. INTRODUCTION

The $Z_2 = 1$ quantum spin hall states and the consequent three-dimensional (3D) strong topological insulators (STI) have attracted great interests since the success in their theoretical predictions and experimental observations.¹⁻⁷ One of the most important reasons is that there exist helical surface states characterized by a full insulating gap and protected by the time-reversal symmetry.^{8,9} Notably, those surface states are spin-momentum locked and exhibit robustness against the nonmagnetic impurities, which makes $Z_2 = 1$ STI an ideal candidate for energy-saving topological devices.

However, there still exist great challenges in the application of $Z_2 = 1$ STI due to their own intrinsic characteristics. Specifically, as a topological device, its on and off status should be controlled, which means the system can be alternated between a conductor and an insulator according to an external field. Since the backscattering is suppressed with nonmagnetic impurities, $Z_2 = 1$ STI is born a perfect conductor. Yet for this reason, it is difficult to realize the off status in $Z_2 = 1$ STI. By now, the most usual manipulation method is to dope magnetic impurities or apply an electromagnetic field,¹⁰⁻¹³ which all encounter the same problems. First, both surfaces of the topological system should be doped in order to induce backscattering, which also makes the system difficult to return to a conductor. Second, since the backscattering only exists where the magnetic impurities or external fields are induced, the surface states can only be controlled locally. However, experimentally, topological insulators usually grow on a substrate, which means any manipulation on a substrate surface becomes nearly impossible due to the difficulty of doping there. Consequently, a nonlocal method to control the surface states close to the substrate in order to build topological devices becomes rather an important topic.

Not long ago, theorists proposed a new kind of $Z_2 = 0$

topological system.¹⁴⁻¹⁷ Considering finite-size effect, the $Z_2 = 0$ topological system with proper size inherits properties of $Z_2 = 1$ STI, besides unique emerging robust helical surface states due to the finite-size confinement. Here, the words “robust” and “emerging” mean those helical surface states are robust against nonmagnetic disorder and only exist in a finite-size system compared to the traditional one. Recently, Zhu et al. found the sign of these $Z_2 = 0$ emerging robust helical surface states in epitaxial Bi(111) thin films.¹⁸ Moreover, in contrast to $Z_2 = 1$ STI, there also exists an unexpected phenomenon that the weak anti-localization peak suddenly disappears after doping magnetic Co on the top surface of thin Bi film. This experiment implies that the surface states on the bottom of thin $Z_2 = 0$ topological system can be manipulated through a nonlocal method on the top surface, which may have great significance in building topological devices.

In this work, we propose a new nonlocal method to build topological devices through the emerging robust helical edge or surface states in $Z_2 = 0$ topological systems. First, we demonstrate the method in a narrow ribbon described by 2D $Z_2 = 0$ anisotropic BHZ model. Without magnetic doping, we find that there exist one pair of emerging robust helical edge states and one pair of gapped normal edge states due to the finite-size confinement. Therefore, the system exhibits conducting characteristics. However, if the top (bottom) of the 2D BHZ model is doped with magnetic impurities, the gapped normal edge states on the bottom (top) gradually become gapless with increasing magnetization. Thus, for moderate magnetization on the top (bottom) edge, the system remains good conductor since there is no backscattering on the bottom (top) edge. When magnetization becomes strong sufficiently, the Anderson disorder can cause strong backscattering on both edges, resulting insulating characteristics for the system. Using the Landauer-Büttiker formula, we verify the above physical

pictures by the two-terminal conductance G , which starts from $2e^2/h$, then maintains at the value of e^2/h , and finally falls to zero. This novel phenomenon enables us to nonlocally manipulate the on and off status in a $Z_2 = 0$ topological system, thus it can also be applied to build new topological devices. Our proposal is also extended to 3D $Z_2 = 0$ topological systems, such as Wilson-Dirac model. And finally, we further discuss the realization of this proposal in Cd_3As_2 type Dirac semimetals.

The rest of this paper is organized as follows. In Sec.II, we first numerically demonstrate this nonlocal engineering method in a 2D anisotropic BHZ model and 3D anisotropic Wilson-Dirac model. Then, we exhibit two detailed plans to build topological devices with $Z_2 = 0$ topological systems. Next, in Sec.III, we generalize this method to more realistic Cd_3As_2 Dirac semimetal materials. Finally, a conclusion is presented in Sec.IV.

II. 2D BHZ MODEL AND 3D WILSON-DIRAC MODEL

We first take the anisotropic BHZ model in square lattice as an example.^{19,20} The four-band tight-binding Hamiltonian in the momentum representation reads:

$$\mathcal{H}(\mathbf{k}) = \begin{pmatrix} H(\mathbf{k}) & 0 \\ 0 & H^*(-\mathbf{k}) \end{pmatrix}$$

$$H(\mathbf{k}) = \tau_z(m - m_x - m_y + m_x \cos k_x + m_y \cos k_y) + \tau_x v_x \sin k_x + \tau_y v_y \sin k_y \quad (1)$$

where m determines the band gap, $v_{x,y}$ reflects the Fermi velocity, and $m_{x,y}$ represents the hopping amplitude between nearest-neighbor sites along the x, y directions, respectively. $\tau_{x,y,z}$ are Pauli matrices representing different orbits. During our calculation, the values of these parameters are chosen as below: $m = 1.64$, $m_x = 0.8$, $m_y = 1.2$, $v_{x,y} = 3$. We consider the ribbon geometry, and the width along y direction is chosen as $L_y = 30a$ (a is the lattice constant) in order to induce finite-size effect.

In this work, our plan of magnetic doping is to dope a soft-magnetic stripe on one edge or surface of the sample. Therefore, the strengths and directions of the magnetic impurities are entirely determined by external magnetic field, and we consider the effect of magnetic impurities in x direction by an adding term $M_x \sigma_x \otimes \tau_0$ on $y = 0$ edge of the ribbon. Actually, even though it will be difficult to accurately control the magnetization strength M_x of the soft-magnetic stripe in experiment, an external magnetic field rotating in x-z direction will also work. Because M_x is determined by $M \cos \theta$, and the existence of M_z has little influence on the final result.

Without magnetic impurities, the energy band of the system is drawn in Fig.1(a), which is double degenerated due to the spin degeneration. There exist two pairs of gapless edge states and two pairs of gapped edge states locating at $k_x = 0$ and $k_x = \pi$, respectively. When the Fermi energy is set $E_F = 0.08$ as the black dashed

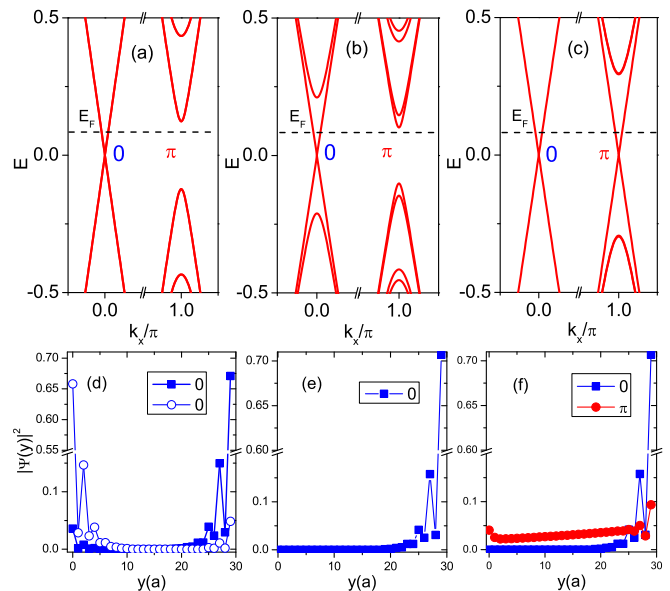


FIG. 1: (Color online) (a)-(c) stand for calculated energy bands in 2D BHZ model with three different strengths of magnetic impurities doped in x direction: $M_x = 0, 1$ and 2.1 , respectively. (d)-(f) represent corresponding probability density distributions of the edge states for (a)-(c) at $E_F = 0.08$, respectively. Only the left propagating states are plotted here.

line shows in Fig.1(a), the corresponding probability density $|\Psi(y)|^2$ is drawn in Fig.1(d). It is obvious that the gapless edge states around $k_x = 0$ mostly locate at two edges, representing the emerging robust helical edge states. Consequently, the edge states around $k_x = \pi$ represent the hybridized gapped normal edge states due to the finite-size confinement.

The energy band with magnetic impurity strength $M_x = 1$ is shown in Fig.1(b). We find that one pair of the previously double degenerated edge states around $k_x = 0$ opens a small gap, while the other one remains close. Moreover, one of the originally double degenerated energy gaps around $k_x = \pi$ becomes smaller. In Fig.1(e), we find that the only existing edge states are the emerging robust helical ones locating at $y = 30a$.

Continuing increasing the impurity strength, the above tendency exhibits much more explicitly. If the impurity strength reaches as strong as $M_x = 2.1$, the smaller gap in Fig.1(b) around $k_x = \pi$ becomes nearly gapless in Fig.1(c). In Fig.1(f), the corresponding probability density $|\Psi(y)|^2$ tells us that the only existing edge states are those locating around $y = 30a$. Specifically, the emerging robust helical edge state colored by blue mostly locates around $y = 30a$, while the normal edge state colored by red extends to inner space, which means it still exhibits properties of bulk states.

In order to quantitatively analysis the physical pictures of energy bands, we further study the transport properties of this system, and calculate the conductance G of this model with nonmagnetic disorder in a two-

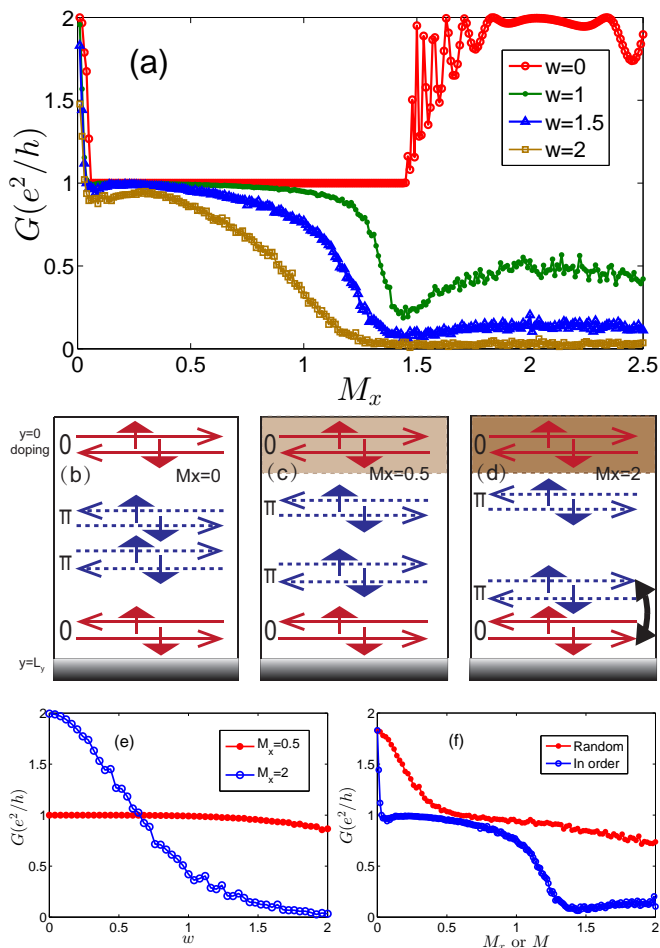


FIG. 2: (Color online) (a) is the conductance G vs M_x for different Anderson disorder strength w in a two-terminal system. The parameters $E_L = E_R = 2.3$ for left and right leads, $E_C = 0.03$ for central part. (b)-(d) are the schematic diagrams corresponding to the three characteristic stages of the conductance in (a) during the process of doping magnetic impurities. (e) is the conductance G vs w with fixed M_x . (f) is the conductance G vs M_x or M for magnetic impurities doped in order or randomly.

terminal system. The nonmagnetic disorder exists inevitably in the realistic system and is modeled by Anderson disorder with random potential uniformly distributed in $[-w/2, w/2]$, where w is the disorder strength. The distance between the two leads is $3000a$ and the Fermi energy of the central region is $E_C = 0.03$. In order to simulate metallic leads at the two terminals, their widths along y direction and Fermi energies are chosen as $N_L = N_R = 200a$ and $E_L = E_R = 2.3$, respectively.

We first show how the conductance varies with the strength of magnetic impurities M_x in Fig.2(a). For the red line without Anderson disorder, the conductance undergoes a transition from $G = 2e^2/h$ to e^2/h , then back to $2e^2/h$. The second plateau of $G = 2e^2/h$ shakes vigorously, because the normal edge states on $y = 30a$ still have properties of bulk states as shown by the red line

in Fig.1(f). The whole transition processes can be understood with the help of the schematic diagrams from Fig.2(b) to 2(d). First, as shown in Fig.2(b), due to the finite-size effect, there exist one pair of emerging robust helical edge states and one pair of gapped normal edge states,¹⁴ while the gapped normal ones have no contribution to the conductance. Therefore, the conductance exhibits $G = 2e^2/h$ at the beginning. Then, in Fig.2(c), if we slightly dope a little amount of magnetic impurities in x direction on $y = 0$ edge, which will induce the backscattering between the counter propagating emerging robust helical edge states on $y = 0$, only the emerging robust helical edge states on $y = L_y$ have contribution to the conductance. Thus, the conductance falls to $G = e^2/h$ fast and then remains unchanged. At last, in Fig.2(d), when M_x is strong sufficiently, the gapped normal edge states on $y = 0$ owns a relatively large gap, and the coupling between the gapped normal edge states on $y = 0$ and $y = L_y$ is really weak. Therefore, the originally gapped normal edge states on $y = L_y$ become gapless and could make contribution to the conductance. As a result, the conductance gets back to $G = 2e^2/h$.

However, considering the inevitable impurities in reality, the system shows exotic transport properties, which is the central result of this paper. If the strength of Anderson disorder is not zero, as shown by the green, blue and brown lines in Fig.2(a), the conductance never returns to $G = 2e^2/h$, but continues falling to nearly zero with strong M_x . This difference can be explained by the backscattering between the emerging robust helical edge states and the normal ones on $y = 30a$ caused by Anderson disorder. The existence of this backscattering is guaranteed by the physical meaning of Z_2 topological invariant: gapless helical edge states with even number are not robust against disorder. Besides, for the green line, when the impurity strength approaches $M_x = 1.5$, we find the conductance exhibits a minimum value during the process of decreasing. This critical point is actually also the transition point from $G = e^2/h$ to $2e^2/h$ without disorder, which means the Fermi energy just touches the bottom of the closing energy band on $k_x = \pi$. In this case, the backscattering in gapped $k_x = \pi$ channel is permitted. Therefore, there exist more backscattering channels shown in Fig.2(d), and the backscattering between the emerging robust helical edge states and the gapped normal ones on $y = 30a$ is somehow enhanced. As a result, the conductance at this point exhibits smaller value than the surrounding points.

Next, let's fix the magnetic impurity strength M_x , and study how the the conductance G varies with Anderson disorder strength w . In Fig.2(e), it is obvious that the conductance with $M_x = 0.5$ exhibits stronger robustness than that with $M_x = 2$, which is consistent with Fig.2(a). Moreover, for instance, if the disorder strength is chosen as $w = 2$, the "on" status of the red line with $M_x = 0.5$ exhibits $G \approx 0.87e^2/h$, while the "off" status of the blue line with $M_x = 2$ exhibits $G \approx 0.03e^2/h$. Therefore, the on-off ratio can be achieved about 30 : 1 in this case.

Till now, we find that by altering the strength of magnetic impurities on one edge, a $Z_2 = 0$ BHZ model with emerging robust helical edge states can be tuned from a perfect one-channel conductor to a perfect insulator, which can be applied to build topological devices.

However, in some cases, it may not be convenient to alter the external field, and the strength of magnetic impurities M_x is fixed. Therefore, let's consider a situation that the direction of doped magnetic impurities is not ordered but in a random arrangement. For simplicity, we just assume that \mathbf{M} is either in x or z direction. During our calculation, $M_x^2 + M_z^2 = M_{total}^2$, $M_x \in [-M_{total}, M_{total}]$, and $M_{total} \in [0, M]$. The red line of Fig.2(f) shows how the conductance varies with magnetic impurity strength M when $w = 1.5$. To have a better comparison, a similar $w = 1.5$ situation with magnetic impurities ordered in x direction is also plotted by a blue line. As we can see, when $M = 2$, the conductance of the red line still maintains at $G \approx 0.8e^2/h$ compared with $G \approx 0.1e^2/h$ of the blue line when $M_x = 2$, which can be regarded as the on and off status of the current. In experiment, this kind of random can be realized in many ways, such as by heating and so on. Therefore, topological devices built by $Z_2 = 0$ 2D BHZ model with emerging robust helical edge states can also be tuned from a perfect one-channel conductor to a perfect insulator by altering the directions of magnetic impurities on one edge.

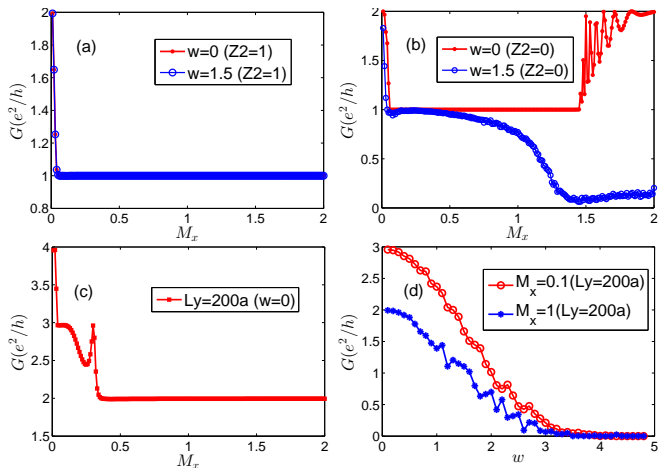


FIG. 3: (Color online) (a): The conductance G vs M_x for $Z_2 = 1$ STI with $m = 1$ in BHZ model. (b): The conductance G vs M_x for $Z_2 = 0$ topological system with $m = 1.64$ in BHZ model. (c): The conductance G vs M_x for $L_y = 200a$ without finite-size effect in BHZ model. (d): The conductance G vs disorder strength w in BHZ model for $L_y = 200a$ without finite-size effect. In (c) and (d), all parameters of the Hamiltonian are chosen the same as Fig.2(a) except L_y .

For further showing the advantages of the above proposals, we also consider a 2D $Z_2 = 1$ BHZ model by changing the parameter m in Eq(1) from 1.64 to 1 and L_y still maintains $30a$. As shown in Fig.3(a), no matter whether there exists Anderson disorder or not, the conductance never falls to zero, but keeps $G = e^2/h$ all

the time. Compared with the $Z_2 = 0$ topological system in Fig.3(b), the $Z_2 = 1$ STI can not turn off the current, which means it is not suitable to build topological devices. Moreover, we also calculate a $Z_2 = 0$ 2D BHZ model without finite-size effect by expanding L_y from $30a$ to $200a$. The red line in Fig.3(c) represents how the conductance G varies with magnetic impurity strength M_x without Anderson disorder, and there exists two characteristic quantum plateaus $G = 3e^2/h$ and $G = 2e^2/h$. In Fig.3(d), we show how the conductance on these two plateaus varies with Anderson disorder strength w . The red line and the blue line represent $M_x = 0.1$ and $M_x = 1$, respectively. Unlike Fig.2(e), the main feature of Fig.3(d) is that the conductances of these two lines start decreasing at the beginning, and fall to zero nearly with the same M_x . This feature tells us that one cannot get high on-off ratio for any disorder strength w or magnetic impurity strength M_x . The reason is that there are always two pairs of gapless helical edge states around $y = L_y$, and the Anderson disorder can cause the backscattering between them (the helical edge states around $k_x = 0$ are no longer emerging robust ones now). Therefore, if we want to switch on or off the current in order to build topological devices just by tuning the strength of doped magnetic impurities on one edge, the existence of $Z_2 = 0$ emerging robust helical edge states due to finite-size confinement is the necessary condition.

Similar phenomenon also exists in 3D $Z_2 = 0$ topological systems, and we take the anisotropic Wilson-Dirac type model as an example.²²⁻²⁷ The Hamiltonian in a cubic lattice reads:

$$\mathcal{H}(\mathbf{k}) = m(\mathbf{k})\sigma_0 \otimes \tau_z + \sum_{\alpha} v_{\alpha} \sin k_{\alpha} \sigma_{\alpha} \otimes \tau_x$$

$$m(\mathbf{k}) = m + \sum_{\alpha} m_{\alpha} (\cos k_{\alpha} - 1) \quad (2)$$

where σ are Pauli matrices in spin space, and $\alpha = x, y, z$. Parameters $\tau, m, v_{\alpha}, m_{\alpha}$ have the same meanings as the 2D model of Eq(1). The width along z direction L_z is chosen as $L_z = 15a$, and the magnetic impurities are doped in z direction on $z = 0$ side. During the calculation, related parameters are chosen as below: $m = 2.26, m_x = 0.9, m_y = 1.1, m_z = 0.8, v_{x,y,z} = 1.5$. In Fig.4(a)-(c), we show how the 3D energy band varies with the strength of doped magnetic impurities $M_z = 0, 1$ and 2 , respectively. There exist two nonequivalent Dirac points $A(C)$ and $B(D)$, and the blue and pink curves represent the two energy bands nearest to the Dirac points. In Fig.4(a), the energy bands locating around $A(C)$ are gapless, because they are the emerging robust helical surface states. However, the appearance of the gaps on $B(D)$ tells us these surface states are the gapped normal ones due to finite-size confinement. In Fig.4(b), $M_z = 1$, we find that the pink curves on $A(C)$, which were gapless at first, now open a small gap, because there exists the backscattering between the counter propagating emerging robust helical surface states on $z = 0$ induced by the magnetic impurities. At last, in Fig.4(c), when the strength of mag-

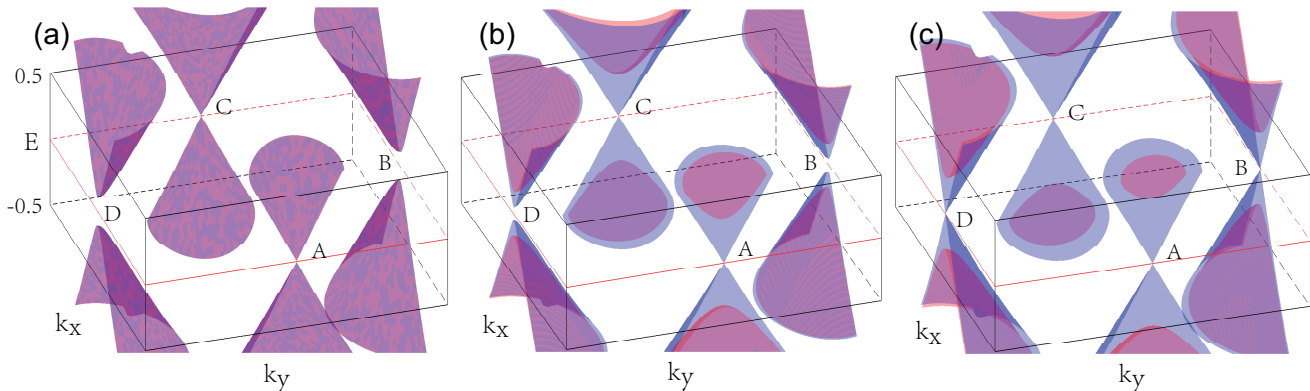


FIG. 4: (Color online) (a)-(c) correspond to the surface energy bands of Wilson-Dirac model with different strengths of magnetic impurities: $M_z = 0, 1$ and 2 , respectively. As M_z increases, one of the two double degenerated gapless surface states on $A(C)$ opens a small gap, while one of the two double degenerated gapped surface states on $B(D)$ gradually becomes gapless.

netic impurities is strong sufficiently, all blue curves at $A(C)$ and $B(D)$ become gapless. Briefly, Dirac points $A(C)$ and $B(D)$ correspond to $k_x = 0$ and $k_x = \pi$ in 2D BHZ model, respectively. And all the physical pictures of Fig.4(a)-(c) are exactly the same as those shown by Fig.1(a)-(c), respectively.

By now, we have afforded two kinds of nonlocal methods to build topological devices in $Z_2 = 0$ topological systems. The first one is to alter the strengths of the doped magnetic impurities. Specifically, we first dope a soft-magnetic film at the top surface of a thin $Z_2 = 0$ topological system grown on a substrate. Then, if we only apply a weak magnetic field on the soft-magnetic film, the whole device is a good conductor. However, if the soft-magnetic film is magnetized strong sufficiently, the whole device turns into an insulator. The second method is to alter the directions of doped magnetic impurities. If the doped magnetic film is magnetized in order with moderate strength, the whole device is an insulator. However, if the magnetic direction of doped magnetic film is in a random arrangement, such as by heating and so on, the whole system gets back to a conductor. Since the above manipulation methods are all nonlocal ones on one edge or surface of the sample, it exhibits great advantages to build topological devices through emerging robust helical surface states in $Z_2 = 0$ topological systems compared with traditional $Z_2 = 1$ STI.

III. EXTENSION TO REAL MATERIALS

Based on above two simple models, we have in principle shown the nonlocal manipulation methods to build topological devices with emerging robust helical surface states in $Z_2 = 0$ topological systems. In this section, let's further extend our proposal to more realistic materials. Though there are several 3D realistic material candidates,^{18,28} we restrict our discussion on 2D cases to avoid the huge computational requirements.

Motivated by the recent theoretical prediction and ex-

perimental realization of Dirac semimetal Cd_3As_2 ,²⁹⁻³¹ we consider a Cd_3As_2 stripe whose effective low energy Hamiltonian $H(\mathbf{k})$ reads as:²⁹

$$H(\mathbf{k}) = \epsilon_0(\mathbf{k}) + \begin{pmatrix} M(\mathbf{k}) & Ak_+ & Dk_- & B^*(\mathbf{k}) \\ Ak_- & -M(\mathbf{k}) & B^*(\mathbf{k}) & 0 \\ Dk_+ & B(\mathbf{k}) & M(\mathbf{k}) & -Ak_- \\ B(\mathbf{k}) & 0 & -Ak_+ & -M(\mathbf{k}) \end{pmatrix} \quad (3)$$

where $\epsilon_0(\mathbf{k}) = C_0 + C_1k_z^2 + C_2(k_x^2 + k_y^2)$, $k_{\pm} = k_x \pm ik_y$, and $M(\mathbf{k}) = M_0 - M_1k_z^2 - M_2(k_x^2 + k_y^2)$ with parameters $M_0, M_1, M_2 < 0$. Since $B(\mathbf{k}) = (\alpha k_z + \beta D)k_z^2$, $B(\mathbf{k})$ can be neglected compared with Dk_{\pm} term if we only consider the expansion up to $O(k^2)$.^{29,32}

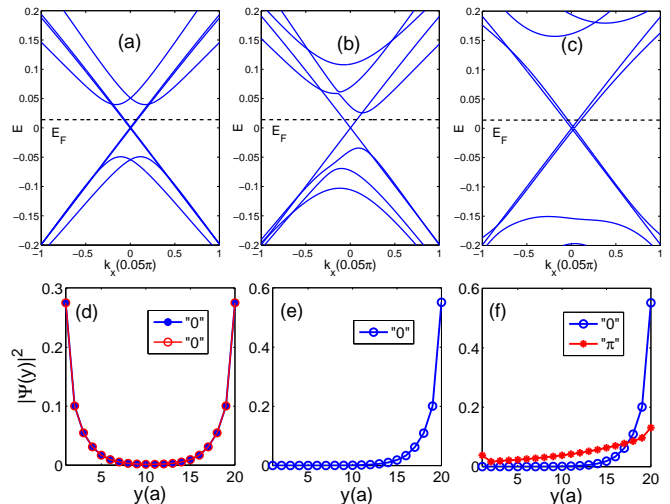


FIG. 5: (Color online) (a)-(c) stand for calculated energy bands in Cd_3As_2 for three different strengths of magnetic impurities doped in x direction: $M_x = 0, 0.2$ and 0.9 , respectively. (d)-(f) are the probability density distributions which has been integrated along z axis for (a)-(c) at $E_F = 0.014$, respectively. In (d)-(f), only the left propagating states are plotted.

In this paper, C_0, C_1 and C_2 are chosen zero, which

can simplify our numerical calculation but has no influence on the physical properties of this model. In fact, main results got from this approximation satisfy realistic Cd_3As_2 materials, though they are not quite true in experiment. Other related parameters are chosen as below: $M_0 = -0.44$, $M_{1,2} = -0.5$, $A = 1.2$, $D = 0.55$. Considering 3D stripe geometry in which $L_z = 6a$ and $L_y = 20a$, the above $\mathbf{k} \cdot \mathbf{p}$ Hamiltonian can be rewritten in tight-binding form, and the energy bands of Cd_3As_2 are drawn in Fig.5(a)-(c). Compared with Fig.1(a)-(c), the two Dirac points $k_x = 0$ and $k_x = \pi$ in BHZ model both locate at $k_x = 0$ with two inverted bands.²⁹ In Fig.5(a), there is no doped magnetic impurity. The two pairs of gapless surface states represent the emerging robust helical ones, and the other two with a visible gap represent the gapped normal ones. Taking the Fermi energy as $E_F = 0.014$, we obtain the distribution of the emerging robust helical surface states in Fig.5(d), and it has been integrated along z axis. As we can see, the red line and blue line seem degenerated, which originates from the coupling between the emerging robust helical surface states on $y = 0$ and $y = 20a$. Next, a little amount of magnetic impurities in x direction ($M_x \sigma_x \otimes \tau_0$) are doped on $y = 0$. In Fig.5(b), we find that one of the two pairs of emerging robust helical surface states opens a small gap, while one of the two pairs of gapped normal surface states tends to close. In this case, the only existing gapless surface states are the emerging robust helical ones concentrating on $y = 20a$ as shown in Fig.5(e). At last, when the strength of magnetic impurities is strong enough, such as Fig.5(c) with $M_x = 0.9$, there exist two pairs of gapless surface states consisting of one pair of emerging robust helical surface states and one pair of normal surface states. The probability density distribution in this case is shown in Fig.5(f). The blue and red lines represent the emerging robust helical surface states and the normal ones, respectively. We find only the surface states concentrating around $y = 20a$ exist now. In fact, every characteristic in Fig.5(a)-(f) of Cd_3As_2 owns its correspondence in Fig.1(a)-(f) of 2D BHZ model, and the physical pictures between these two models are exactly the same.

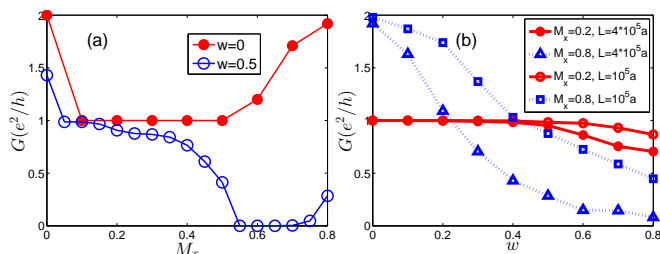


FIG. 6: (Color online) (a): The red and blue lines stand for the conductance G vs M_x in Cd_3As_2 for two Anderson disorder strengths $w = 0$ and $w = 0.5$, respectively. (b): The red and blue lines stand for the conductance G vs w in Cd_3As_2 for two fixed magnetic impurity strengths $M_x = 0.2$ and 0.8 , respectively.

Finally, we also calculate the conductance of Cd_3As_2 with Anderson-type disorder in a two-terminal system. The Fermi energies of the two leads and the central part are $E_L = E_R = 0.5$ and $E_C = 0.01$, respectively. Without loss of generality, the disorder is only added on the $y = 20a$ boundary.³³ Fig.6(a) tells us how the conductance varies with the strength of magnetic impurities M_x . In the red line, there is no Anderson disorder and the distance between the two leads is $4 \times 10^5 a$. Similar to 2D BHZ model, the conductance falls to a plateau of $G = e^2/h$ from the beginning $G = 2e^2/h$ rapidly, and then goes back to $G = 2e^2/h$. However, if the disorder strength is chosen $w = 0.5$ shown by the blue line, the conductance decreases from $G = 2e^2/h$ to $G = e^2/h$, and never goes back to $G = 2e^2/h$ but continues falling to nearly zero. Similar as the green line in Fig.2(a), a critical point around $M_x = 0.6$ also exists, but exhibits much more explicit than that in BHZ model. According to the conductance behavior under moderate disorder strength $w = 0.5$, we can claim the two-terminal device is in “on” status when $M_x \in [0.1, 0.3]$ and in “off” status when $M_x > 0.55$. In order to better understand the performance of the topological device, we also show how the conductance varies with Anderson disorder strength w with fixed magnetic impurity strength M_x in Fig.6(b). When the device is in the claimed “off” status (such as $M_x = 0.8$), the conductance G quickly falls to zero with the increasing disorder strength w . In contrast, when the device is in the claimed “on” status (such as $M_x = 0.2$), the conductance nearly maintains at $G = e^2/h$, no matter how the disorder strength w or the length of the strip changes. According to Fig.6(b), a relatively high on-off ratio about 10 : 1 is obtained when $w > 0.4$, which is suitable for the topological devices. Moreover, the stronger the disorder strength is and the longer the stripe is, the higher the on-off ratio can be obtained. Nevertheless, disorder strength can not be too strong in case of the broken of the “on” status. In fact, Fig.6(b) is consistent with Fig.2(e), which is also the result of finite-size effect and the key to switch on or off the current by doping magnetic impurities on one surface.

To summarize, all conclusions obtained from 2D BHZ model can also be found in Cd_3As_2 type Dirac semimetals, which generalizes our proposals building new topological devices to a much broader prospect.

IV. CONCLUSION

In conclusion, we show that in $Z_2 = 0$ topological systems, one can switch on and off the current nonlocally just by doping magnetic impurities on one edge or surface of the sample, which enables us to build topological devices through emerging robust helical surface states in $Z_2 = 0$ topological systems. This proposal is first demonstrated in 2D $Z_2 = 0$ anisotropic BHZ model and 3D Wilson-Dirac type model in detail. Notably, it is also generalized to realistic Cd_3As_2 type Dirac semimetals.

Since the manipulation methods proposed here are all nonlocal ones, $Z_2 = 0$ topological system with emerging robust helical surface states exhibits much brighter prospects in building topological devices than the traditional $Z_2 = 1$ STI.

ACKNOWLEDGMENTS

This work was financially supported by MOST of China (Grant No. 2012CB821402), NBRPC (Grant

No. 2014CB920901), NSFC (Grants Nos. 91221302, 11374219, 11204065(JTS), and 11474085(JTS)), and the NSF of Jiangsu province BK20130283.

-
- * jianghuaphy@suda.edu.cn
- ¹ M. Z. Hasa and C. L. Kane, *Rev. Mod. Phys.* **82**, 3045 (2010); X.-L. Qi and S.-C. Zhang, *Rev. Mod. Phys.* **83**, 1057 (2011); Y. Ando, *J. Phys. Soc. Jpn.* **82**, 102001 (2013).
 - ² C. L. Kane and E. J. Mele, *Phys. Rev. Lett.* **95**, 226801 (2005); **95**, 146802 (2005).
 - ³ M. König, S. Wiedmann, C. Brüne, A. Roth, H. Buhmann, L. W. Molenkamp, X.-L. Qi and S.-C. Zhang, *Science* **318**, 766 (2007).
 - ⁴ H.-J. Zhang, C.-X. Liu, X.-L. Qi, X. Dai, Z. Fang and S.-C. Zhang, *Nat. Phys.* **5**, 438 (2009).
 - ⁵ D. Hsieh, Y. Xia, L. Wray, D. Qian, A. Pal, J. H. Dil, J. Osterwalder, F. Meier, G. Bihlmayer, C. L. Kane, Y. S. Hor, R. J. Cava and M. Z. Hasan, *Science* **323**, 919 (2009).
 - ⁶ T. Hanaguri, K. Igarashi, M. Kawamura, H. Takagi and T. Sasagawa, *Phys. Rev. B* **82**, 081305(R) (2010).
 - ⁷ Y. L. Chen, J. G. Analytis, J.-H. Chu, Z. K. Liu, S.-K. Mo, X. L. Qi, H. J. Zhang, D. H. Lu, X. Dai, Z. Fang, S. C. Zhang, I. R. Fisher, Z. Hussain and Z.-X. Shen, *Science* **325**, 178 (2009).
 - ⁸ D. Hsieh, Y. Xia, D. Qian, L. Wray, F. Meier, J. H. Dil, J. Osterwalder, L. Patthey, A. V. Fedorov, H. Lin, A. Bansil, D. Grauer, Y. S. Hor, R. J. Cava and M. Z. Hasan, *Phys. Rev. Lett.* **103**, 146401 (2009).
 - ⁹ T. Zhang, P. Cheng, X. Chen, J.-F. Jia, X. Ma, K. He, L. Wang, H. Zhang, X. Dai, Z. Fang, X.C. Xie and Q.-K. Xue, *Phys. Rev. Lett.* **103**, 266803 (2009).
 - ¹⁰ Y. Okada, C. Dhital, W. Zhou, E. D. Huemiller, H. Lin, S. Basak, A. Bansil, Y.-B. Huang, H. Ding, Z. Wang, S. D. Wilson and V. Madhavan, *Phys. Rev. Lett.* **106**, 206805 (2011).
 - ¹¹ L. A. Wray, S.-Y. Xu, Y. Xia, D. Hsieh, A. V. Fedorov, Y. S. Hor, R. J. Cava, A. Bansil, H. Lin and M. Z. Hasan, *Nat. Phys.* **7**, 32 (2011).
 - ¹² H. Li, R. Shen, L. B. Shao, B. Wang, D. N. Sheng and D. Y. Xing, *Phys. Rev. Lett.* **110**, 266802 (2013).
 - ¹³ X. Qian, J. Liu, L. Fu, B. Wang and J. Li, *Science* **346**, 1344 (2014).
 - ¹⁴ H. Jiang, H. Liu, J. Feng, Q. Sun and X.C. Xie, *Phys. Rev. Lett.* **112**, 176601 (2014).
 - ¹⁵ H. Guo, L. Yang and S.-Q. Shen, *Phys. Rev. B* **90**, 085413 (2014).
 - ¹⁶ B. d. Leeuw, C. Küppersbusch, V. Juričić and L. Fritz, arXiv:1411.0255v1.
 - ¹⁷ T. Fukui and Y. Hatsugai, arXiv:1501.07031v3.
 - ¹⁸ K. Zhu, L. Wu, X. Gong, S. Xiao, S. Li, X. Jin, M. Yao, D. Qian, M. Wu, J. Feng, Q. Niu, F.d. Juan and D.-H. Lee, arXiv:1403.0066v1.
 - ¹⁹ B. A. Bernevig, T. L. Hughes and S.-C. Zhang, *Science* **314**, 1757 (2006).
 - ²⁰ X.-L. Qi, Y. S. Wu and S.-C. Zhang, *Phys. Rev. B* **74**, 085308 (2006).
 - ²¹ B. Zhou, H.-Z. Lu, R.-L. Chu, S.-Q. Shen and Q. Niu, *Phys. Rev. Lett.* **101**, 246807 (2008); H.-Z. Lu, W.-Y. Shan, W. Yao, Q. Niu and S.-Q. Shen, *Phys. Rev. B* **81**, 115407 (2010).
 - ²² K.-I. Imura, M. Okamoto, Y. Yoshimura, Y. Takane and T. Ohtsuki, *Phys. Rev. B* **86**, 245436 (2012).
 - ²³ R. S. K. Mong, J. H. Bardarson and J. E. Moore, *Phys. Rev. Lett.* **108**, 076804 (2012).
 - ²⁴ Z. Ringel, Y. E. Kraus and A. Stern, *Phys. Rev. B* **86**, 045102 (2012).
 - ²⁵ K. Kobayashi, T. Ohtsuki and K.-I. Imura, *Phys. Rev. Lett.* **110**, 236803 (2013).
 - ²⁶ Y. Yoshimura, A. Matsumoto, Y. Takane and K.-I. Imura, *Phys. Rev. B* **88**, 045408 (2013).
 - ²⁷ C.-X. Liu, X.-L. Qi, H.-J. Zhang, X. Dai, Z. Fang, and S.-C. Zhang, *Phys. Rev. B* **82**, 045122 (2010).
 - ²⁸ X. Li, F. Zhang, Q. Niu and J. Feng, *Sci. Rep.* **4**, 6387 (2014).
 - ²⁹ Z. Wang, H. Weng, Q. Wu, X. Dai and Z. Fang, *Phys. Rev. B* **88**, 125427 (2013).
 - ³⁰ M. Neupane, S.-Y. Xu, R. Sankar, N. Alidoust, G. Bian, C. Liu, I. Belopolski, T.-R. Chang, H.-T. Jeng, H. Lin, A. Bansil, F. Chou and M. Z. Hasan, *Nat. Commun.* **5**, 3786 (2014).
 - ³¹ S. Borisenko, Q. Gibson, D. Evtushinsky, V. Zabolotnyy, Bernd Büchner and R. J. Cava, *Phys. Rev. Lett.* **113**, 027603 (2014).
 - ³² S. Jeon, B. B. Zhou, A. Gyenis, B. E. Feldman, I. Kimchi, A. C. Potter, Q. D. Gibson, R. J. Cava, A. Vishwanath and A. Yazdani, *Nat. Mater.* **13**, 851 (2014).
 - ³³ Since the boundary contacts the outside environment directly, the disorder on the boundary should be stronger than that in the inner space. Moreover, in 2D BHZ model, we have demonstrated that the proposed effect exists even though the disorder is added in the whole system. In Cd_3As_2 Dirac semimetal materials, we also found the existence of this effect, and we just consider this approximate condition to make the effect more explicit.